Neuro-Oncology

Neuro-Oncology 18(1), 87–95, 2016
doi:10.1093/neuonc/nov128
Advance Access date 22 July 2015

The effects of anti-angiogenic therapy on the formation of radiation-induced microbleeds in normal brain tissue of patients with glioma†

Janine M. Lupo, Annette M. Molinaro, Emma Essock-Burns, Nicholas Butowski, Susan M. Chang, Soonmee Cha, and Sarah J. Nelson

Department of Radiology and Biomedical Imaging, University of California San Francisco, San Francisco, California (J.M.L., E.E.-B., S.C., S.J.N.); Department of Neurosurgery, University of California San Francisco, San Francisco, California (A.M.M., N.B., S.M.C., S.C.); Department of Epidemiology and Biostatistics, University of California San Francisco, San Francisco, California (A.M.M.); Department of Bioengineering and Therapeutic Sciences, University of California San Francisco, San Francisco, California (S.J.N.)

†This work was presented in part at the 19th annual meeting of ISMRM, Montreal, Canada 2011, and the 16th annual meeting of SNO, Garden Grove, California, USA.

Corresponding Author: Janine M. Lupo, PhD, Byers Hall UCSF, Box 2532, 1700 4th Street, Suite 303, San Francisco, CA 94158 (janine.lupo@ucsf.edu).

Background. Radiotherapy (RT) is an integral component in managing patients with glioma, but the damage it may cause to healthy brain tissue and quality of life is of concern. Susceptibility-weighted imaging (SWI) is highly sensitive to the detection of microbleeds that occur years after RT. This study's goals were to characterize the evolution of radiation-induced microbleeds in normal-appearing brain and determine whether the administration of an anti-angiogenic agent altered this process.

Methods. Serial high-resolution SWI was acquired on 17 patients with high-grade glioma between 8 months and 4.5 years post-treatment with RT and adjuvant chemotherapy. Nine of these patients were also treated with the anti-angiogenic agent enzastaurin. Microbleeds were identified as discrete foci of susceptibility not corresponding to vessels, tumor, or postoperative infarct, and counted in normal-appearing brain. Analysis of covariance was performed to compare slopes of regression of individual patients' microbleed counts over time, Wilcoxon rank-sum tests examined significant differences in rates of microbleed formation between groups, and linear and quadratic mixed-effects models were employed.

Results. The number of microbleeds increased with time for all patients, with initial onset occurring at 8–22 months. No microbleeds disappeared once formed. The average rate of microbleed formation significantly increased after 2 years post-RT ($P < .001$). Patients receiving anti-angiogenic therapy exhibited fewer microbleeds overall ($P < .05$) and a significant reduction in initial rate of microbleed appearance ($P = .01$).

Conclusions. We have demonstrated a dramatic increase in microbleed formation after 2 years post-RT that was decelerated by the concomitant administration of anti-angiogenic therapy, which may aid in determining brain regions susceptible to RT.

Keywords: anti-angiogenic therapy, glioma, microbleeds, radiation therapy, susceptibility-weighted imaging, treatment effects.

Although radiation therapy (RT) is an integral component in the management of patients with glioma, the damage that it may cause to healthy brain tissue function and impact upon quality of life is of concern.[1] Because of the diffuse boundaries and infiltrative nature of gliomas, surgical resection rarely results in removal of all tumor tissue. As a result, standard of care for residual disease for patients with high-grade glioma involves RT with adjuvant chemotherapy with the aim of impeding growth of residual tumor. Conventional RT utilizes external beam radiation planning to deliver a total dose of 60 Gy in 30 fractions over a course of 6 weeks. Despite attempts to minimize radiation dose to normal tissue, the surrounding healthy brain tissue may receive upward of 30 Gy 10 cm away from the tumor perimeter. Even with modern technology, ~60% of tissue within the high-dose treatment field is normal brain tissue.[2] Since modern RT delivery technologies now allow for spatially selective, modulated treatment plans, it is of utmost importance to identify the underlying pathogenic mechanisms

Received 24 March 2015; accepted 12 June 2015
© The Author(s) 2015. Published by Oxford University Press on behalf of the Society for Neuro-Oncology. All rights reserved. For permissions, please e-mail: journals.permissions@oup.com.

Downloaded from https://academic.oup.com/neuro-oncology/article/18/1/87/2509142 by guest on 24 April 2024

of brain injury and find biological correlates that can measure these changes noninvasively. It has been reported that many glioma survivors experience a progressive decline in neurocognitive function after irradiation.[1] Gaining insight into the pathogenesis of treatment-related brain injury and having an objective means for evaluating the extent and severity of these effects so that they can be integrated into the management of patient care is especially critical for patients with grade II and III gliomas, who have longer survival times and earlier age of onset.

At a microscopic level, the histologic response to radiation initially shows characteristic vascular changes and white matter pathology ranging from demyelination to coagulative necrosis, as well as cortical atrophy and endothelial proliferation.[3] In studies that have used physiological MRI techniques to characterize the early effects of RT on normal brain, changes in blood-vessel permeability, diffusivity, and fractional anisotropy values were observed in irradiated brain tissue 2–4 months after the completion of RT.[4–7] After 6 months post-RT, increases in T2-hyperintensity have been found in irradiated temporal lobes,[8] and dose-dependent changes in diffusivity values within the parahippocampal cingulum and temporal lobe white matter have been directly associated with subsequent neurocognitive deficits.[9] T2*-weighted, phase-sensitive imaging has indicated long-term vasculopathy, with progressive impairment in cerebral microcirculation and the formation of microbleeds and vascular malformations such as cavernous angiomas.[10,11] The clinical manifestation of these events usually begins anywhere from 9 months to several years after receiving RT, followed by presentation of obvious neurological deterioration many months or even years later that compromises the patient's quality of life.[12]

Besides improving the delivery of RT in order to minimize toxicity, there has been research into the pharmacologic manipulation of the tumor and brain vasculature, which may influence the efficacy and toxicity of ionizing radiation.[13] For example, the concomitant administration of anti-angiogenic agents (AAs) has been shown to protect normal tissue from radiation toxicity.[14–16] The combination of bevacizumab, a monoclonal antibody that disrupts the pathway of vascular endothelial growth factor, and hypo-fractionated stereotactic RT has been reported to improve the therapeutic ratio of radiation by reducing the number of side effects and toxicity in heavily pretreated patients, protecting against radiation necrosis and the need for additional corticosteroid use during or after radiation.[15] Radiation necrosis, which results from increasing capillary permeability caused by cytokine release that leads to extracellular edema, can also be minimized or reversed by blocking vascular endothelial growth factor, thereby decreasing the vascular permeability.[16]

Susceptibility-weighted imaging (SWI) is a powerful tool for detecting microbleeds[17,18] that have been observed in several studies involving stroke and vasculopathy-related injury using this technique.[18–24] In a prior study, we used SWI to evaluate the long-term effects of RT on normal-appearing brain tissue in 20 patients with gliomas and demonstrated that microbleeds appeared in irradiated patients after 2 years from receiving therapy, that the prevalence of these lesions increased over time since receiving RT, and that they often extended outside the T2-lesion volume and into the contralateral hemisphere.[11] Microbleeds were not observed in patients who were only treated with chemotherapy. The lack of serial imaging data in that study meant that there was limited information available to describe the initial evolution of these lesions.

The primary goal of the current study was to use SWI to characterize the evolution of microbleeds in normal-appearing brain tissue that form within the first 5 years following RT on an individual patient basis. Since anti-angiogenic drugs are thought to have a radioprotective effect on the existing vasculature,[14–16] our second aim was to determine whether the concomitant administration of an AA altered the process of microbleed formation due to irradiation. It is hypothesized that microbleeds will initially appear at a slower rate, which will then increase over time, and patients who received an AA will develop fewer microbleeds.

Materials and Methods

Patient Population

Seventeen patients with high-grade glioma based on World Health Organization criteria were retrospectively examined in this study. All patients underwent surgical resection followed by a standard 6-week cycle of 30 fractions of external beam RT and temozolomide (75 mg/m^2 daily during RT and 200 mg/m^2 for 5 days every 28-day cycle after RT). In order to enroll in the study, patients were required to have a Karnofsky performance score of $\geq$70 and provide informed consent in accordance with guidelines established by our institutional review board. One patient was excluded from the analysis due to rapid increase in microbleeds before 2 years post-RT that were far away from the site of the tumor, and thought to be due to another origin. In the remaining 16 patients analyzed, 6 had diagnoses of grade III and 10 had grade IV glioma. Patient age range at the time of RT was 25–66 years, with a median age of 43. Six patients were on medication for hypertension. Half of the patients (all glioblastoma multiforme [GBM]) also received concomitant and adjuvant anti-angiogenic therapy, consisting of the protein kinase C inhibitor enzastaurin (250 mg daily). The clinical details for each patient are listed in Table 1. Patients were divided into 2 groups, RT and RT + AA (Table 2). A minimum of 2 exams between 9 months and 4.5 years following the onset of RT were evaluated for every patient.

MR Imaging Acquisition

Patients were serially scanned on a 3T EXCITE scanner (GE Healthcare Technologies) with an 8-channel head coil (MRI Devices) between 8 and 50 months after beginning RT. High resolution T2*-weighted SWI was acquired using a 3D flow-compensated spoiled gradient echo (SPGR) sequence with echo time (TE)/repetition time (TR) of 28 ms/56 ms, 20-degree flip angle, 24 cm field of view (FOV), 512 × 144 image matrix with GRAPPA (generalized autocalibrating partially parallel acquisition) R = 2 plus 16 autocalibrating lines, and an in-plane resolution of 0.5 × 0.5 mm with 2 mm slice thickness. Standard clinical pre- and postcontrast T1-weighted SPGR images (TR = 8.86 ms, TE = 2.50 ms, matrix = 256 × 256, slice thickness = 1.5 mm, FOV = 24 × 24 cm, inversion time = 400 ms, flip

Downloaded from https://academic.oup.com/neuro-oncology/article/18/1/87/2509142 by guest on 24 April 2024

Table 1. Summary of clinical data for each patient

Patient	Tumor Grade	Tumor Type	Age	Gender	Tumor Location	Therapy Group	KPS	Hypertension Status
1	III	Astro	30	F	Frontal	RT	90	N
2	III	Oligo	34	F	Parietal	RT	80	N
3	IV	GBM	46	F	Temporal	RT	80	N
4	III	Oligo	45	F	Frontal	RT	90	N
5	II	Epend	30	M	Brainstem	RT	80	Y
6	IV	GBM	66	F	Parietal	RT	90	Y
7	III	Astro	31	M	Frontal	RT	80	N
8	III	Oligo	39	M	Frontal	RT	100	N
9	IV	GBM	45	M	Frontal	RT + AA	90	Y
10	IV	GBM	42	M	Occipital	RT + AA	90	N
11	IV	GBM	41	M	Frontal	RT + AA	90	Y
12	IV	GBM	55	F	Parietal	RT + AA	80	N
13	IV	GBM	55	F	Frontal	RT + AA	80	Y
14	IV	GBM	25	M	Frontal	RT + AA	90	N
15	IV	GBM	56	F	Parietal	RT + AA	90	Y
16	IV	GBM	56	M	Temporal	RT + AA	90	UK

Abbreviations: astro, astrocytoma; oligo, oligodendroglioma; epend, ependymoma; Y, on medication for hypertension; N, no record of hypertension; UK, unknown.

Table 2. Description of patient groups

Group	# of Patients	Total # of Scans	# of Scans/Patient	
			Median	Range
RT	8	26	3	2–5
RT + AA	8	39	4	2–11

angle = 15 degrees) were also acquired for defining anatomic regions of interest.

Image Processing

Images were transferred to a Linux workstation (Sun Microsystems). The SWI processing employed a 72×72 Hanning filter, and the resulting phase mask was multiplied with the magnitude T2*-weighted image 4 times. A lowpass filter with edge completion was applied to the combined images, and minimum intensity projections through 8-mm thick slabs were generated to obtain the final SW images used for analysis.[21] Phase images were also generated to confirm the absence of calcification in these lesions. Standard clinical pre- and postcontrast T1-SPGR images were used to exclude regions within acute hemorrhage and contrast-enhancing tumor, respectively, from the analysis. These images were registered to the SWI through rigid body transformations that maximized the normalized mutual information.[25]

Image and Statistical Analysis

Microbleeds were identified as discrete foci of susceptibility that did not correspond to vessels, tumor, or border surgical cavity on consecutive slices. The number of microbleeds was counted in normal-appearing tissue, outside the tumor region and any areas of acute hemorrhage. In order to minimize user error from counting, microbleeds from each dataset were labeled and iteratively counted multiple times, until the same number of counts was obtained from 2 consecutive trials as performed by Lupo et al.[11] The maximum number of iterations required for all patients was 4, and the counter was blinded to the date of RT. The resulting data were plotted as function of time since RT. Changes in microbleed morphology were qualitatively assessed.

All statistical analyses were performed using R software, version 2.9.2 (www.r-project.org). Simple linear regression was first employed to assess global differences in microbleed formation over time before and after 2 years from RT. An analysis of covariance (ANCOVA) was performed to compare the slopes of the regression lines between these 2 groups. Linear mixed effects models were also employed to model serial data from individual patients as a random effect, first for each group individually, and then combined with each group modeled as a fixed effect. This type of regression analysis was performed to associate microbleed count with time since RT for 2 sets of patient groupings: (i) prior to versus after 2 years from the start of RT, and (ii) with and without concomitant anti-angiogenic therapy. A Wilcoxon rank-sum test was then utilized to test for significant differences in individual rates of microbleed formation between populations for each of these groupings. In order to assess overall differences in microbleed count over time between therapy groups, microbleed counts were first binned into 1-year intervals for each therapy group. A Kruskal–Wallis rank-sum test was implemented to test for significant differences between therapy groups at each year. To model the observed quadratic effect of time, a quadratic time-dependent model analysis was subsequently implemented. No formal adjustment of type I error was undertaken due to the

Downloaded from https://academic.oup.com/neuro-oncology/article/18/1/87/2509142 by guest on 24 April 2024

exploratory nature of the study; in all cases, $P < .05$ was considered statistically significant.

Results

Rate of Microbleed Formation

As expected based on previously published data,[11] the number of microbleeds increased with time in all patients. For the 9 patients who had received SWI scans every 2 months during the first 2 years, the initial onset of microbleed appearance ranged from 8 to 22 months (median 13 mo). No microbleeds disappeared once formed. As shown in Fig. 1B, a 4-fold increase in median rate of microbleed formation was observed after 2 years from receiving RT compared with before 2 years since starting RT. This was evident by both an increase in the slope of the regression line for all patients from 2.1 to 16.9 when grouped together (Fig. 1A) and a statistically significant increase in the median rate of formation from 3.7 to 15.8 microbleeds/year when patients were analyzed individually ($P < .001$; Fig. 1B). Although a trend was clearly observed (Fig. 1A), microbleed count was not significantly associated with time since RT ($R^2 = 0.06$, $P = .08$) before 2 years post-RT when not taking into account serial data from different patients individually, while beyond 2 years post-RT, a statistically significant association was found between microbleed count and time ($R^2 = 0.83$, $P < .0001$). However, when modeling individual patients as a random effect, significant associations were found between microbleed count and time since RT for both the before 2 years post-RT group ($P = .0004$, Fig. 1C) and the after 2 years post-RT group ($P < .00001$, Fig. 1D). No relationship was found between patient age and microbleed formation, and no differences in microbleed formation were found between patients who had a history of hypertension compared with those who did not.

Effects of Anti-angiogenic Therapy on Microbleed Formation

Patients treated with anti-angiogenic therapy exhibited fewer microbleeds overall. During the first 2 years after

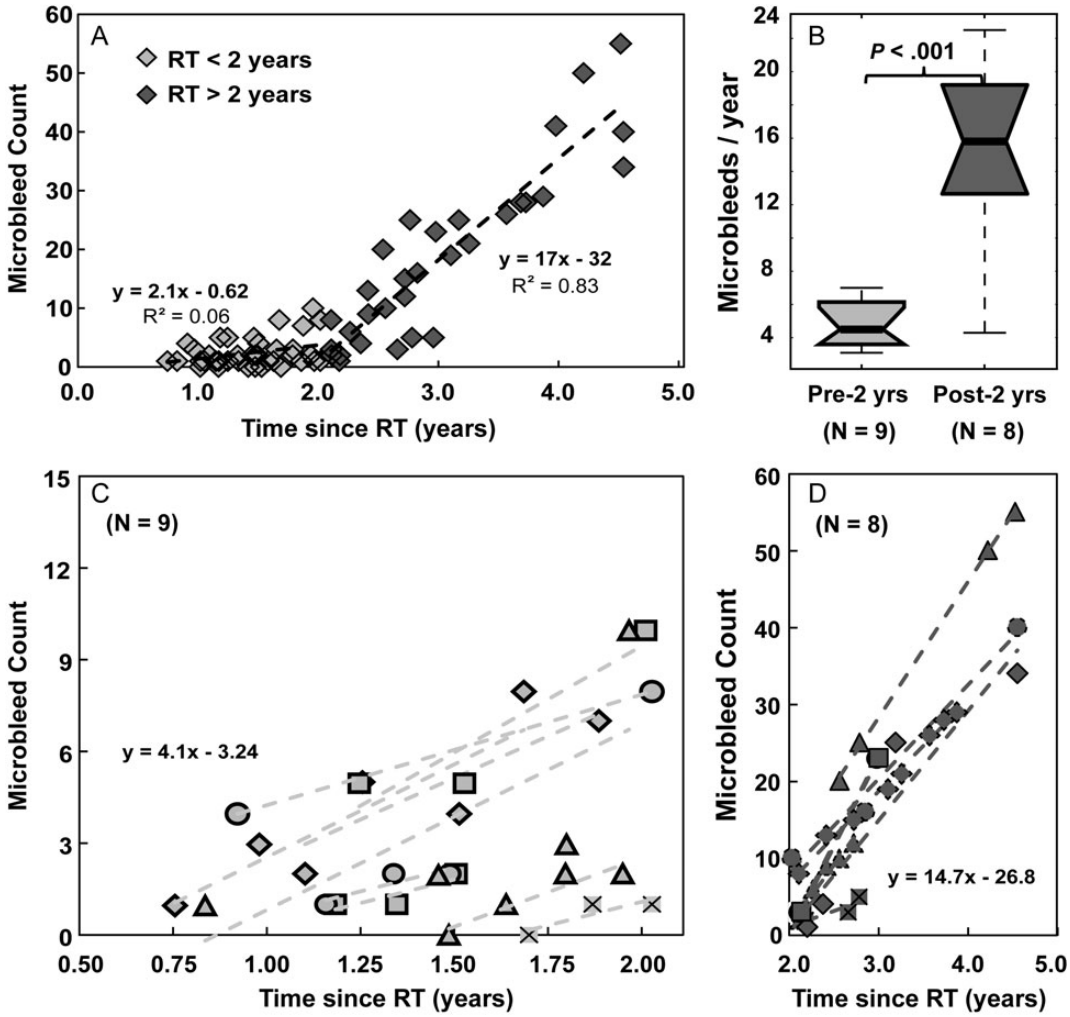

Fig. 1. Serial assessment of microbleed formation. (A) Microbleed counts from all patient exams plotted as a function of time since RT. (B) Box plots of rates of microbleed formation pre-2 years vs post-2 years from the start of RT. (C) Evolution of microbleed appearance for individual patients in the first 2 years after receiving RT. (D) Evolution of microbleed appearance for individual patients between 2 and 5 years after receiving RT.

Downloaded from https://academic.oup.com/neuro-oncology/article/18/1/87/2509142 by guest on 24 April 2024

receiving RT, the RT + AA group had significantly fewer microbleeds over time ($P < .01$, Fig. 2A) and a significant reduction in the initial rate of microbleed appearance ($P < .05$; Fig. 2B) compared with the RT group. Although a trend in reduced microbleed formation was observed with anti-angiogenic therapy after 2 years post-RT, there was no difference between the RT and RT + AA groups when employing linear models (Fig. 2C and D). Because of the small number of patients with imaging at later time points, the differences between therapy groups were subsequently characterized over all time points together. When microbleed counts were binned over 1-year intervals (Fig. 3A), no significance between the RT and RT + AA groups was observed for any of the individual paired bins. However, when the differences between the 2 therapy groups over all time points were assessed using a time-dependent quadratic mixed effects model, the RT + AA group overall had significantly fewer microbleeds ($P < .05$, Fig. 3B).

Qualitative Assessment of Individual Microbleed Characteristics

No trends between microbleed size and onset were found. Three types of microbleeds were observed, as shown in Fig. 4: (i) stable: remaining the same size once they appear (Fig. 4A); (ii) enlarging: increasing in size over time (Fig. 4B); and (iii) large and stable: initially appearing with a diameter of several millimeters and then remaining that size (Fig. 4C). Individual patients in either group could possess any combination of these types of microbleeds. Some microbleeds appeared in locations where there was no prior visible vasculature, while others directly stemmed from the deterioration of a larger neighboring vessel (Fig. 4D).

Discussion

Fractionated RT remains part of the standard treatment for all patients with newly diagnosed grade III and grade IV gliomas

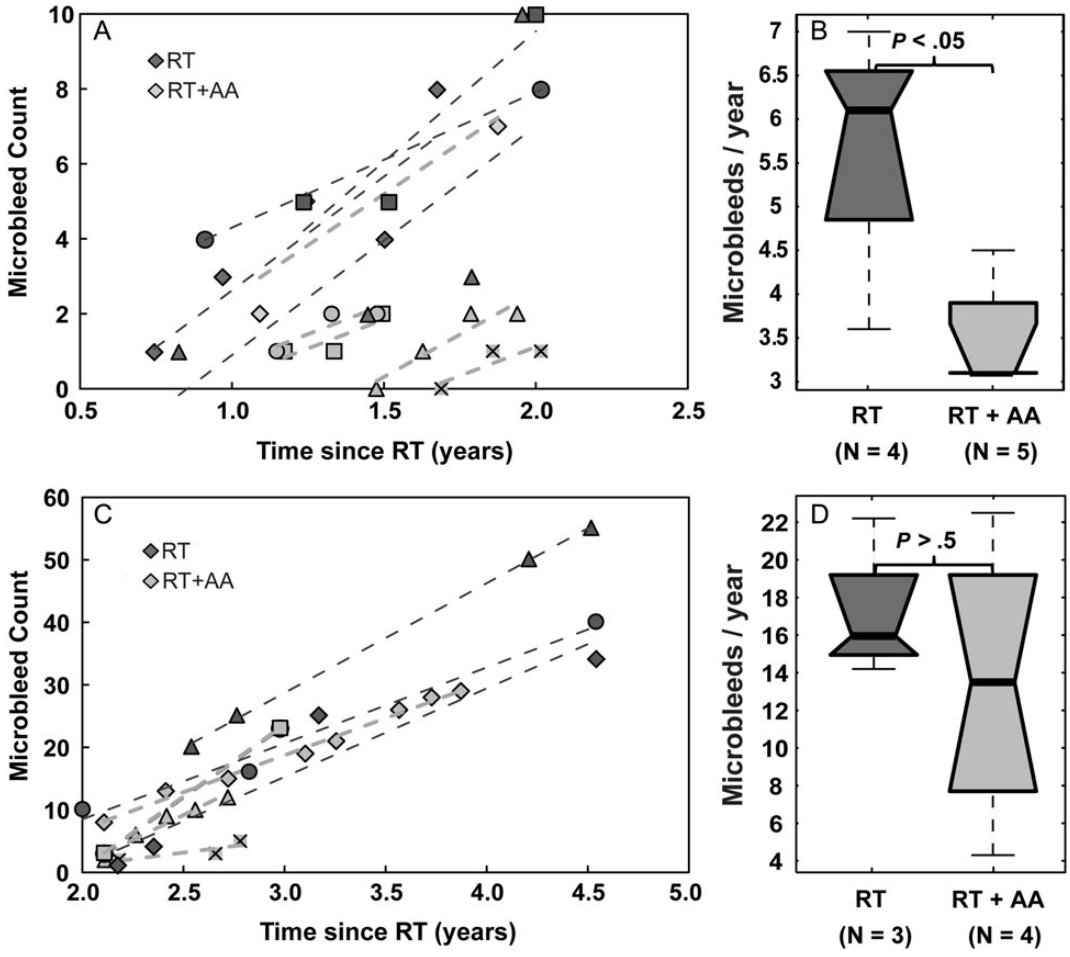

Fig. 2. Effects of anti-angiogenic therapy on microbleed formation. (A) Evolution of microbleed appearance in the first 2 years after receiving RT for individual patients who received anti-angiogenic therapy (light gray, RT + AA) compared with those who did not (dark gray, RT). (B) Box plots of rates of microbleed formation in the first 2 years for patients who did and did not receive anti-angiogenic therapy during the course of RT. (C) Evolution of microbleed appearance between 2 and 5 years post- RT for individual patients who received anti-angiogenic therapy (light gray, RT + AA) compared with those who did not (dark gray, RT). (D) Box plots of rates of microbleed formation between 2 and 5 post-RT years for patients who did and did not receive anti-angiogenic therapy during the course of RT.

Downloaded from https://academic.oup.com/neuro-oncology/article/18/1/87/2509142 by guest on 24 April 2024

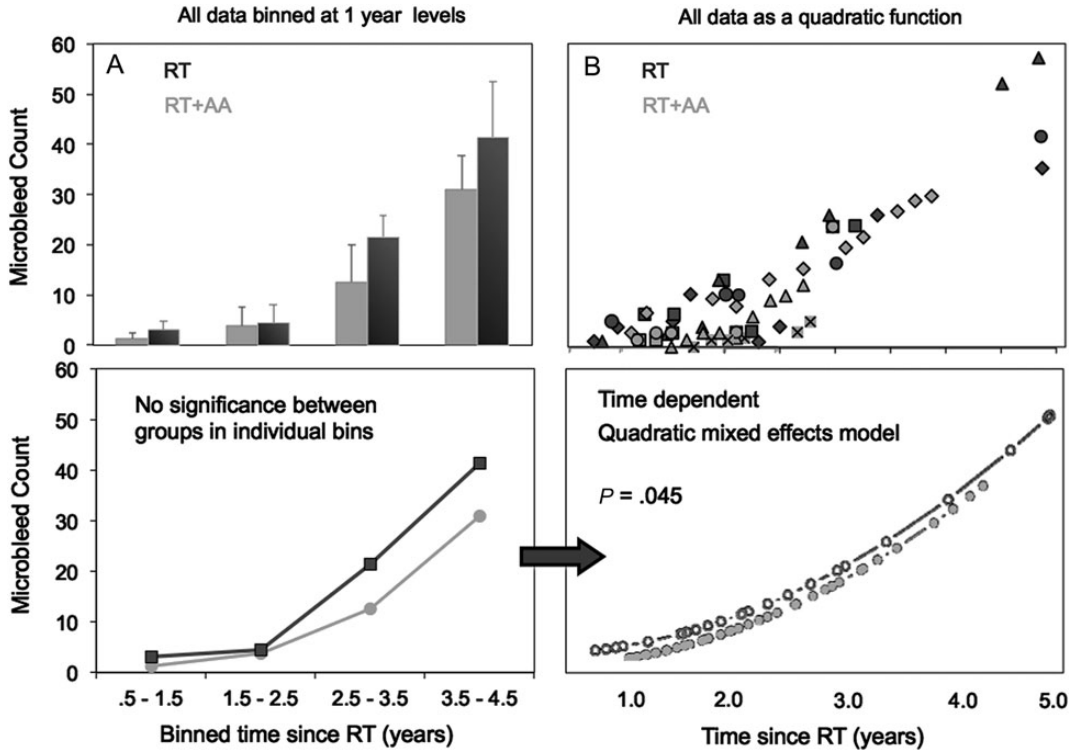

Fig. 3. Effects of anti-angiogenic therapy on microbleed formation over time. (A) All data binned at 1-year intervals illustrating a clear trend in increase in microbleed count over time and more microbleeds present in the RT group, even though no significant difference was found between therapy groups at each time window. (B) All data (top panel) modeled as a quadratic mixed effects model (bottom panel) showing a significant difference in microbleed counts over time between treatment groups.

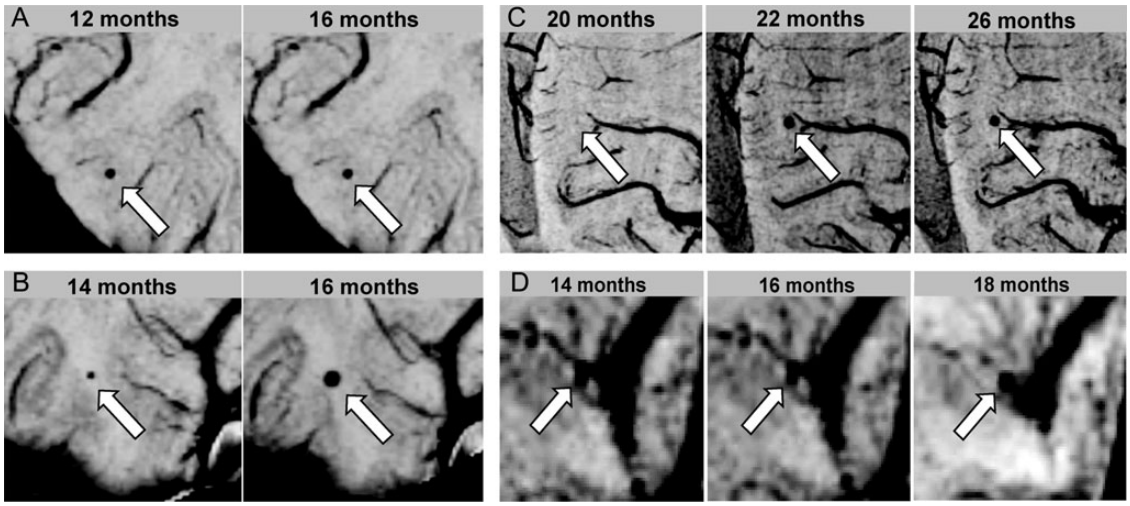

Fig. 4. Types of microbleeds. (A) *Stable*: microbleeds that remain the same size over time once they appear. (B) *Enlarging*: microbleeds that increase in size over time. (C) *Large and stable*: microbleeds that initially appear with a diameter of several millimeters and then remain that size. (D) Example of a microbleed that directly stems from the deterioration of a larger neighboring vessel.

after surgical resection and also may be used in patients with grade II glioma. Although our prior study was able to show an increase in the number of microbleeds with time from RT, the lack of serial imaging data meant that there was limited information available to describe the initial evolution of these lesions. The primary goal of the current study was to use SWI to characterize the evolution of microbleeds in normal-appearing brain tissue that result from RT on an individual

Downloaded from https://academic.oup.com/neuro-oncology/article/18/1/87/2509142 by guest on 24 April 2024

patient basis. Our ability to capture patients at regular intervals at earlier time points in this study allowed us to further characterize the initial onset and rate of microbleed formation compared with prior studies. This study design was able to elucidate how, in adults, microbleeds initially appear at a very slow rate and then, after 2 years post-onset of RT, suddenly begin to increase as time progresses. Individual patients formed microbleeds at different rates, which can in part explain the variability observed in our previous analysis where each time point was obtained from a different patient.[11] Although an increasing trend was observed with microbleed formation and time from RT, when all patients were grouped together a significant association did not exist in the current study until after 2 years. However, when individual patients were modeled as a random effect, significant associations between microbleed count and time since RT were observed both before and after 2 years from the onset of RT.

In an attempt to understand why microbleeds formed faster in some patients than in others, we investigated the effects of age and hypertension status on microbleed formation. Consistent with previous reports in both irradiated adults and children,[11,26] age was not associated with rate of microbleed formation at any time, nor was the time of onset, even though the presence of cerebral microbleeds in adults with neurodegenerative and cerebral vascular disease has been shown to increase with age.[27] We believe that the present observation is due to the fact that 88% of our patients were between the ages of 30 and 60 at the time of RT. In irradiated children, microbleeds have been shown to appear as early as 5 months, with a much larger variability in rate of formation and faster rates than we have observed in adults.[26] A second potential confounding factor is hypertension status, as positive associations between hypertension status and microbleed count have been reported in the literature.[28,29] However, in our study there was no difference in the rate of microbleed formation between patients who had a history of hypertension and those who did not. Of the patients who received concomitant anti-angiogenic therapy, 50% had a history of hypertension compared with only 25% in the RT group. The AA group was also on average 7 years older and all had a diagnosis of GBM. All of these factors should make patients in the AA group at higher risk for developing microbleeds compared with the RT group, yet they had fewer microbleeds.

Since anti-angiogenic drugs are thought to have a radioprotective effect on the existing vasculature,[14–16] our second aim was to determine whether the concomitant administration of an AA altered the process of microbleed formation due to irradiation. Despite the fact that these agents have not shown survival benefits when used as upfront therapies, there is evidence that they can delay progression and improve quality of life.[30] Although there have been several studies investigating the potential combinatory effects of an AA and RT in preventing radiation necrosis by decreasing vascular permeability and reducing hypoxia, they focus on the tumor and/or surrounding tissue that receives high doses of RT (>45 Gy).[14,31,32] The effects of middle (30–45 Gy) and lower (<30 Gy) doses of radiation on human vasculature in normal-appearing brain tissue are vastly understudied, both in animal models and in vivo. Our observation that patients who received an anti-angiogenic therapy developed fewer microbleeds over time is consistent with the existing hypothesis that anti-angiogenic drugs may have a radioprotective effect on microvasculature by slowing down the process of radiation-induced injury; however, the mechanism by which this occurs, the spatial distribution of microbleeds throughout the brain, the relationship to radiation dose received, and impact on cognitive outcome still need to be explored.

The most significant limitation of the current study design was the small number of patient scans available at later time points, which was in part due to the poor survival of patients with GBM. Although retrospective analysis facilitated our ability to obtain SWI data from 5 of 10 patients with GBM well over 2.5 years after diagnosis when median survival is only 1.5 years, our comparison of therapy groups 2 years following RT was most affected by the fact that we were underpowered, precluding significance. To overcome this issue, however, we employed a quadratic mixed effects model that incorporated the data from all time points, allowing the result to reach statistical significance. Although more variation was observed at later time points, overall smaller standard deviations were found in this study compared with data from a matched time range in our prior study, likely due to the narrower window in which the RT was performed. Despite the presumed more similar RT delivery technology utilized, there were still differences in the extent of radiation dose received to healthy brain tissue that were likely to contribute to the variation we observed. In an attempt to determine whether tumor size prior to radiation (as a rough estimate of treatment volume) had an effect on rate of microbleed formation in the first 2 years, we correlated the volume of residual tumor (enhancing and non-enhancing) plus the resection cavity for 5 RT + AA patients who had a baseline, pre-RT MRI exam; however, no trend was observed.

Methodologically, the main limitation of this study was the potential for error in microbleed identification. The high conspicuity of both veins and microbleeds makes it challenging to accurately separate microbleeds from perpendicular veins using automated methods. Although care was taken to avoid these vessels by examining consecutive slices above and below the plane of each microbleed, misidentification of perpendicular veins as microbleeds was possible. The contiguous slice coverage of the 3D scan and minimum-intensity projections limited this source of error, and other studies[33] have demonstrated that this error is typically consistent across different exams for the same reviewer. Our equivalent acquisition parameters and processing pipeline among all scans, as well as full supratentorial brain coverage, decreased the likelihood of imprecision in microbleed identification.

In conclusion, we have demonstrated that the appearance of microbleeds increases as a function of time since receiving RT. After 2 years, the rate of microbleed formation increases nearly 4-fold compared with microbleeds that appear before 2 years post-RT. The addition of an AA appeared to slow down this process. The size of the microbleeds varied both within and across patients with time. The ability to characterize the evolution of these lesions in normal brain tissue may be important in determining which parts of the brain are most susceptible to RT, and in further understanding the utility of such treatment in patients with lower-grade tumors, who have relatively long survival. Future studies will focus on quantifying the size and spatial distribution of these lesions over time,

Downloaded from https://academic.oup.com/neuro-oncology/article/18/1/87/2509142 by guest on 24 April 2024

correlating with radiation dose and presence of neurocognitive deficits, and replicating findings in a larger, prospective cohort with other anti-angiogenic therapies.

Funding

This study was supported by NIH grants R01-CA059880 and P50-CA97257, and a Joelle Syverson American Brain Tumor Association Fellowship.

Acknowledgments

The authors would like to thank Angela Jakary, Adam Elkhaled, Trey Jalbert, Shauna O'Donnell, Bert Jimenez, Mary McPolin, Jason Crane, and Beck Olson of the Department of Radiology and Biomedical Imaging at UCSF for their assistance with post-processing issues, scanning, or data collection regarding this manuscript.

Conflict of interest statement. None declared.

References

1. Karim AB, Afra D, Cornu P, et al. Randomized trial on the efficacy of radiotherapy for cerebral low-grade glioma in the adult: European Organization for Research and Treatment of Cancer Study 22845 with the Medical Research Council study BRO4: an interim analysis. *Int J Radiat Oncol Biol Phys*. 2002;52(2):316–324.
2. Park I, Tamai G, Lee MC, et al. Patterns of recurrence analysis in newly diagnosed glioblastoma multiforme after three-dimensional conformal radiation therapy with respect to pre-radiation therapy magnetic resonance spectroscopic findings. *Int J Radiat Oncol Biol Phys*. 2007;69(2):381–389.
3. Valk PE, Dillon WP. Radiation injury of the brain. *AJNR Am J Neuroradiol*. 1991;12(1):45–62.
4. Lee MC, Cha S, Chang SM, et al. Dynamic susceptibility contrast perfusion imaging of radiation effects in normal-appearing brain tissue: changes in the first-pass and recirculation phases. *J Magn Reson Imaging*. 2005;21(6):683–693.
5. Weitzner M. Psychosocial and neuropsychiatric aspects of patients with primary brain tumors. *Cancer Invest*. 1999;17(4):285–291; discussion 296–297.
6. Nagesh V, Tsien CI, Chenevert TL, et al. Radiation-induced changes in normal-appearing white matter in patients with cerebral tumors: a diffusion tensor imaging study. *Int J Radiat Oncol Biol Phys*. 2008;70(4):1002–1010.
7. Chapman CH, Nazem-Zadeh M, Lee OE, et al. Regional variation in brain white matter diffusion index changes following chemoradiotherapy: a prospective study using tract-based spatial statistics. *PLoS One*. 2013;8(3):e57768. Epub 2013 Mar 4.
8. Wang YX, King AD, Zhou H, et al. Evolution of radiation-induced brain injury: MR imaging-based study. *Radiology*. 2010;254(1):210–218.
9. Chapman CH, Nagesh V, Sundgren PC, et al. Diffusion tensor imaging of normal-appearing white matter as biomarker for radiation-induced late delayed cognitive decline. *Int J Radiat Oncol Biol Phys*. 2012;82(5):2033–2040. Epub 2011 May 11.
10. Jain R, Robertson PL, Gandhi D, et al. Radiation-induced cavernomas of the brain. *AJNR Am J Neuroradiol*. 2005;26(5):1158–1162.
11. Lupo JM, Chuang CF, Chang SM, et al. 7-Tesla susceptibility-weighted imaging to assess the effects of radiotherapy on normal-appearing brain in patients with glioma. *Int J Radiat Oncol Biol Phys*. 2012;82(3):e493–e500. Epub 2011 Oct 12.
12. DeAngelis LM, Delattre JY, Posner JB. Radiation-induced dementia in patients cured of brain metastases. *Neurology*. 1989;39(6):789–796.
13. McGee MC, Hamner JB, Williams RF, et al. Improved intratumoral oxygenation through vascular normalization increases glioma sensitivity to ionizing radiation. *Int J Radiat Oncol Biol Phys*. 2010;76(5):1537–1545.
14. Zachary I. Neuroprotective role of vascular endothelial growth factor: signalling mechanisms, biological function, and therapeutic potential. *Neurosignals*. 2005;14:207–221.
15. Gutin PH, Iwamoto FM, Beal K, et al. Safety and efficacy of bevacizumab with hypofractionated stereotactic irradiation for recurrent malignant gliomas. *Int J Radiat Oncol Biol Phys*. 2009;75(1):156–163. Epub 2009 Jan 23.
16. Matuschek C, Bölke E, Nawatny J, et al. Bevacizumab as a treatment option for radiation-induced cerebral necrosis. *Strahlenther Onkol*. 2011;187(2):135–139. Epub 2011 Jan 24.
17. Haacke EM, Xu Y, Cheng YC, et al. Susceptibility weighted imaging (SWI). *Magn Reson Med*. 2004;52(3):612–618.
18. Haacke EM, DelProposto ZS, Chaturvedi S, et al. Imaging cerebral amyloid angiopathy with susceptibility-weighted imaging. *AJNR Am J Neuroradiol*. 2007;28(2):316–317.
19. Akter M, Hirai T, Hiai Y, et al. Detection of hemorrhagic hypointense foci in the brain on susceptibility-weighted imaging clinical and phantom studies. *Acad Radiol*. 2007;14(9):1011–1019.
20. Haacke EM, Cheng NY, House MJ, et al. Imaging iron stores in the brain using magnetic resonance imaging. *Magn Reson Imaging*. 2005;23(1):1–25. Review.
21. Lupo JM, Banerjee S, Hammond KE, et al. GRAPPA-based susceptibility-weighted imaging of normal volunteers and patients with brain tumor at 7 T. *Magn Reson Imaging*. 2009;27(4):480–488.
22. Barnes SR, Haacke EM. Susceptibility-weighted imaging: clinical angiographic applications. *Magn Reson Imaging Clin N Am*. 2009;17(1):47–61.
23. Hermier M, Nighoghossian N. Contribution of susceptibility-weighted imaging to acute stroke assessment. *Stroke*. 2004;35(8):1989–1994.
24. Santhosh K, Kesavadas C, Thomas B, et al. Susceptibility weighted imaging: a new tool in magnetic resonance imaging of stroke. *Clin Radiol*. 2009;64(1):74–83. Review. Erratum in: Clin Radiol. 2009 Jun;64(6):653.
25. Studholme C, Hill D, Hawkes D. An overlap invariant entropy measure of 3D medical image alignment. *Pattern Recognition*. 1999;32:71–86.
26. Peters S, Pahl R, Claviez A, et al. Detection of irreversible changes in susceptibility-weighted images after whole-brain irradiation of children. *Neuroradiology*. 2013;55(7):853–859. Epub 2013 Apr 16.
27. Shams S, Martola J, Granberg T, et al. Cerebral microbleeds: different prevalence, topography, and risk factors depending on dementia diagnosis: the Karolinska Imaging Dementia Study. *AJNR Am J Neuroradiol*. 2015;36(4):661–666.
28. Liu W, Liu R, Sun W, et al. Different impacts of blood pressure variability on the progression of cerebral microbleeds and white matter lesions. *Stroke*. 2012;43(11):2916–2922. Epub 2012 Sep 4.

Downloaded from https://academic.oup.com/neuro-oncology/article/18/1/87/2509142 by guest on 24 April 2024

29. Sun J, Soo YO, Lam WW, et al. Different distribution patterns of cerebral microbleeds in acute ischemic stroke patients with and without hypertension. *Eur Neurol*. 2009;62(5):298–303. Epub 2009 Aug 29.

30. Henriksson R, Asklund T, Poulsen HS. Impact of therapy on quality of life, neurocognitive function and their correlates in glioblastoma multiforme: a review. *J Neurooncol*. 2011;104(3): 639–646. Epub 2011 Apr 6.

31. Liu D, Cao G, Cen Y, et al. The radiosensitizing effect of CpG ODN107 on human glioma cells is tightly related to its antiangiogenic activity via suppression of HIF-1α/VEGF pathway. *Int Immunopharmacol*. 2013;17(2):237–244. Epub 2013 Jun 19.

32. Wachsberger P, Burd R, Dicker AP. Tumor response to ionizing radiation combined with antiangiogenesis or vascular targeting agents: exploring mechanisms of interaction. *Clin Cancer Res*. 2003;9(6):1957–1971.

33. Bian W, Banerjee S, Kelly DA, et al. Simultaneous imaging of radiation-induced cerebral microbleeds, arteries and veins, using a multiple gradient echo sequence at 7 Tesla. *J Magn Reson Imaging*. 2014 Dec 4 [Epub ahead of print]. doi: 10.1002/jmri.24802.

Downloaded from https://academic.oup.com/neuro-oncology/article/18/1/87/2509142 by guest on 24 April 2024